

Rotating quantum droplets confined in a harmonic potential

S. Nikolaou¹, G. M. Kavoulakis^{1,2}, and M. Ögren^{2,3}

¹*Hellenic Mediterranean University, P.O. Box 1939, GR-71004, Heraklion, Greece*

²*HMU Research Center, Institute of Emerging Technologies, GR-71004, Heraklion, Greece*

³*School of Science and Technology, Örebro University, 70182 Örebro, Sweden*

(Dated: November 14, 2023)

We investigate the rotational properties of a two-component, two-dimensional self-bound quantum droplet, which is confined in a harmonic potential and compare them with the well-known problem of a single-component atomic gas with contact interactions. For a fixed value of the trap frequency, choosing some representative values of the atom number, we determine the lowest-energy state, as the angular momentum increases. For a sufficiently small number of atoms, the angular momentum is carried via center-of-mass excitation. For larger values, when the angular momentum is sufficiently small, we observe vortex excitation instead. Depending on the actual atom number, one or more vortices enter the droplet. Beyond some critical value of the angular momentum, however, the droplet does not accommodate more vortices and the additional angular momentum is carried via center-of-mass excitation in a “mixed” state. Finally, the excitation spectrum is also briefly discussed.

PACS numbers: 03.75.Lm, 05.30.Jp, 67.85.-d

I. INTRODUCTION

The rotational properties of trapped atomic Bose-Einstein condensates is a problem which has been studied very extensively in the last decades. Most of these studies have been performed in a harmonic potential, since this has been by far the most common form of confining potential that is used in experiments. We stress that the literature on this problem is very extensive, so we simply refer to some review articles [1–5].

The interatomic interactions are modeled as an effective hard-core potential. This potential is proportional to the so-called scattering length, which describes the elastic, s-wave atom-atom collisions. In the single-component condensates, when this effective interaction is repulsive (i.e., the scattering length is positive), as the angular momentum increases, vortices enter the cloud from its periphery and eventually a vortex lattice forms. When the angular momentum increases even more, the system reaches the so-called limit of “rapid rotation”, where the mean-field approximation fails. The cloud enters a highly correlated regime, and its many-body state resembles a (bosonic) Laughlin-like state. On the other hand, when the effective interaction is attractive (i.e., the scattering length is negative), the cloud is unstable against collapse if there is no trapping potential. Still, the system may be in a metastable state due to the trap. In this case, the cloud carries its angular momentum via center-of-mass excitation of the ground (nonrotating) state.

More recently Petrov [6] predicted in the case of a two-component Bose-Einstein condensate the existence of “quantum droplets”. This is a very interesting problem and has attracted a lot of attention, see, e.g., the review articles [7, 8], and Refs. [9–34]. Interestingly enough, such droplets have been observed experimentally not only in two-component Bose-Einstein condensed gases [35–39] but also in single-component gases with strong dipolar interactions [40–45].

The basic idea in the case where droplets are formed

from binary mixtures is that, due to the fact that we have a two-component system, by tuning the strength of the effective interaction between the same and different components, the mean-field interaction energy may become as small as we wish. In this case the next-to-leading-order correction of the energy (i.e., the so-called “Lee-Huang-Yang” term) [46], becomes comparable with the usual mean-field term and the two terms may balance each other, giving rise to self-bound droplets, even in the absence of any trapping potential.

Self-bound droplets belong to the class of systems which are superfluid. It is thus natural to examine their rotational properties. Compared with the problem of single-component atomic Bose-Einstein condensates, there are two main differences, which introduce novel effects in their superfluid properties. First of all, as we saw earlier, while quantum droplets are self-bound and do not require any trapping potential, in the case of single-component atomic condensates, the presence of a confining potential is absolutely necessary. Second, in quantum droplets, the sign of the nonlinear term depends on the density, being attractive for sufficiently low densities and repulsive, for higher densities. On the other hand, in single-component condensates the interaction is modeled as a hard-core potential and it is either (purely) repulsive, or (purely) attractive.

As we explain below, the question of how a quantum droplet carries angular momentum is essentially trivial when there is no external confining potential. On the other hand, it becomes novel and interesting when the droplet is confined in a trapping potential [20, 27]. This is precisely the problem that we investigate below. More specifically, we consider a harmonically trapped two-dimensional “symmetric” droplet. This consists of two components, however, due to the symmetry between them, the problem reduces to a single order parameter which is common to both of them. We minimize the energy under a fixed expectation value of the total angular momentum $L\hbar$, and a fixed value of the total atom number N of the two components of the droplet.

According to the results of our study, the combination of a (harmonic) trapping potential with the more “complex” nonlinear term introduces a very serious difference in the rotational response of a droplet, as compared with the case of contact interactions. For a sufficiently small N the droplet executes center-of-mass rotation. For larger N and small L the droplet develops surface waves and eventually a single vortex enters the droplet. With increasing L , depending on the value of N more vortices may enter the cloud, up to some critical value of L . Beyond this value, it is no longer energetically favorable for the droplet to accommodate more vortices. The additional angular momentum is then carried via center-of-mass excitation, in a “mixed” state.

In Sec. II we present the model that we use. Then, in Sec. III we present and analyze our results for some representative values of N and various values of L . In Sec. IV we present the general picture that results from our analysis. In Sec. V we present some results from the excitation spectrum that we have found. In Sec. VI we investigate the experimental relevance of our results. Finally, in Sec. VII we summarize the main results of our study and compare the present problem with the “traditional” one, i.e., that of a single-component with an (attractive, or repulsive) effective contact interaction.

II. MODEL

In what follows below we work with dimensionless units. In Sec. VI we restore the units in order to make contact with experimentally relevant parameters. Assuming that there is a very tight confining potential along the axis of rotation, we consider motion of the atoms in the perpendicular plane, i.e., two-dimensional motion. We also assume that the quantum droplet is confined in a two-dimensional harmonic potential

$$V(\rho) = \frac{1}{2}\omega^2\rho^2, \quad (1)$$

where ω is the frequency of the harmonic potential and ρ is the radial coordinate in cylindrical-polar coordinates.

As mentioned also above, we consider the “symmetric” case, where the scattering lengths for the elastic atom-atom collisions between the same species are assumed to be equal for the two components. Also, both the masses of the two species, as well as the densities of the two components are equal. In this case the system is described by a single order parameter $\Psi(\rho, \theta)$, where θ is the angle in cylindrical-polar coordinates. Working with fixed L and N , we minimize the following extended energy functional, [47] which, in dimensionless units, takes the form [9, 29]

$$\begin{aligned} \mathcal{E}(\Psi, \Psi^*) &= \\ &= \int \left(\frac{1}{2}|\nabla\Psi|^2 + \frac{1}{2}\omega^2\rho^2|\Psi|^2 + \frac{1}{2}|\Psi|^4 \ln \frac{|\Psi|^2}{\sqrt{e}} \right) d^2\rho \\ &\quad - \mu \int \Psi^* \Psi d^2\rho - \Omega \int \Psi^* \hat{L} \Psi d^2\rho. \end{aligned} \quad (2)$$

In the above equation Ψ is normalized to the number of atoms, $\int |\Psi|^2 d^2\rho = N$. Also, \hat{L} is the operator of the angular momentum, while μ and Ω are Lagrange multipliers, corresponding to the conservation of the atom number and of the angular momentum, respectively.

The corresponding nonlinear equation that $\Psi(\rho, \theta)$ satisfies is

$$\left(-\frac{1}{2}\nabla^2 + \frac{1}{2}\omega^2\rho^2 + |\Psi|^2 \ln |\Psi|^2 - \Omega \hat{L} \right) \Psi = \mu \Psi. \quad (3)$$

III. ROTATIONAL BEHAVIOR OF THE DROPLET FOR VARIOUS VALUES OF THE ATOM NUMBER

A. Ground state of the droplet in the absence and in the presence of a harmonic potential

To understand the rotational properties of a quantum droplet in the presence of a harmonic confining potential, first of all, let us recall that in the absence of any trapping potential the droplet carries its angular momentum via center-of-mass excitation of the ground (nonrotating) state, since this is a self-bound state [27].

For the discussion that follows it is also useful to recall that in the absence of a harmonic potential and in the Thomas-Fermi limit, we have the so-called “flat-top” droplet. The energy per particle of the droplet is, in this case,

$$\frac{E}{N} = \frac{N}{2\pi\rho_0^2} \ln \frac{N}{\sqrt{e}\pi\rho_0^2} = \frac{\bar{n}}{2} \ln \frac{\bar{n}}{\sqrt{e}}, \quad (4)$$

where we have introduced the “mean” (two-dimensional) density $\bar{n} = N/(\pi\rho_0^2)$. The value of the mean density of the droplet that minimizes the energy (which is also equal to the density of the “flat-top” droplet, assumed to be constant) is $\bar{n} = N/(\pi\rho_0^2) = 1/\sqrt{e} \approx 0.607$, while the corresponding minimum energy per particle is equal to $-1/(2\sqrt{e}) \approx -0.303$.

In the presence of a harmonic potential, in addition to the size of the droplet ρ_0 that we introduced above, we also have the oscillator length $a_{\text{osc}} = 1/\sqrt{\omega}$. If the size of the droplet is much smaller than the oscillator length, $\rho_0 \ll a_{\text{osc}}$ (i.e., for sufficiently small values of N , or ω), we still have center-of-mass excitation. We stress at this point that a unique feature of the harmonic potential is that the center-of-mass coordinate decouples from the relative coordinates, which is crucial for the results presented below [48–50]. In the opposite limit, $\rho_0 \gg a_{\text{osc}}$ (i.e., for sufficiently large values of N , or ω), the rotational properties of the droplet are determined by the harmonic potential, where singly quantized vortices carry the angular momentum.

Let us get an estimate about how N and ω relate in the cross-over regime. From the expression $\rho_0 = [N/(\pi\sqrt{e})]^{1/2}$ that we mentioned above, which is valid in the Thomas-Fermi regime with no external potential, in order for ρ_0 to be equal to a_{osc} , $N\omega \approx \pi\sqrt{e} \approx 5.18$.

We minimized numerically the functional of Eq. (2) using the damped second-order in fictitious time method,

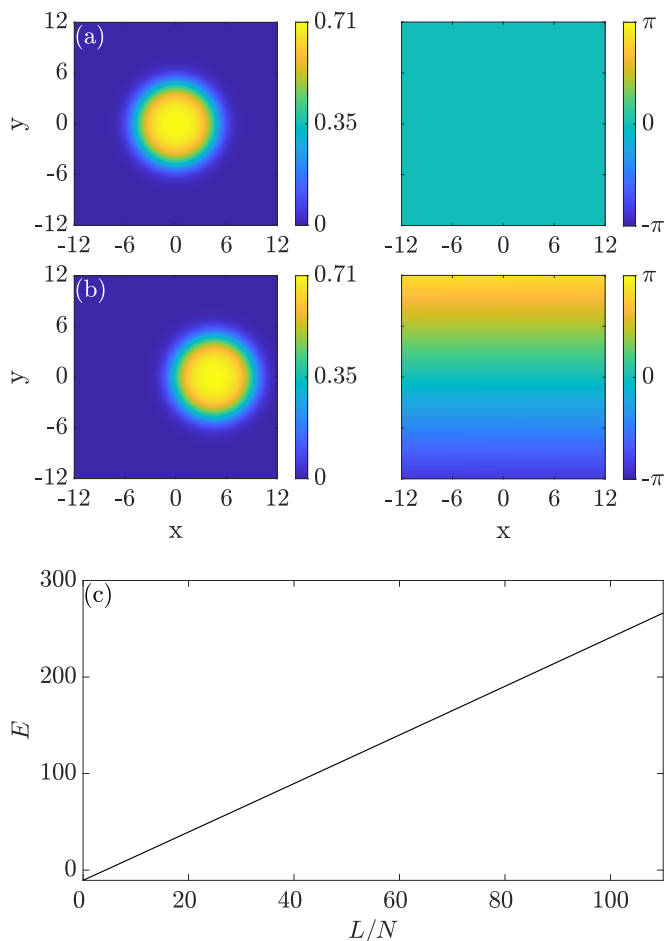


FIG. 1: [(a), (b)] The density (left column, in units of Ψ_0^2) and the phase (right column) of the droplet order parameter, in the lowest-energy state, for $N = 50$, $\omega = 0.05$, and $L/N = 0.0$ and 1.0 , respectively. The unit of length is x_0 . (c) The corresponding dispersion relation, i.e., $E = E(L/N)$. The unit of energy is E_0 and the unit of angular momentum is \hbar .

described in Ref. [47], which is a method of constrained minimization. In the calculations that we performed, a square spatial grid was used, with $\delta x = \delta y = 0.1$. We checked that the choice of this grid step size gives results that are converged with respect to the grid resolution. We stress that the actual size of the domain in the calculations was larger than shown in the figures, to avoid boundary effects. For each value of the angular momentum, a variety of states was used as initial conditions, to ensure that the calculation converged to the lowest-energy state. First, the initial condition for each value of angular momentum was chosen to be the converged solution for the previous value of the angular momentum, e.g., for $L/N = 2.8$ the initial condition was chosen to be the converged solution for $L/N = 2.6$. In addition to that, we repeated the calculations with different initial conditions, using states that represent center-of-mass excitation, surface-wave excitation, vortex excitation and linear combinations of these. The convergence of the calculation to the same solution for the majority of the chosen initial conditions was a strong indication

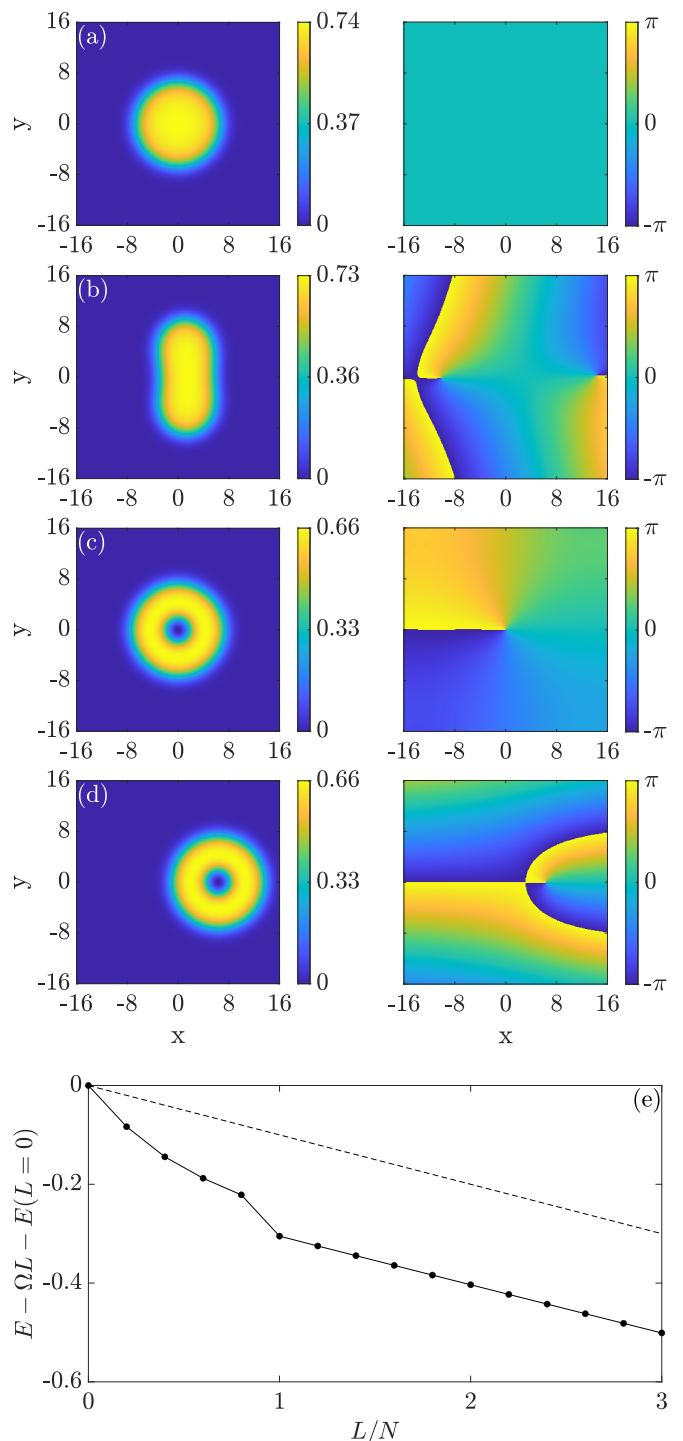


FIG. 2: [(a)–(d)] The density (left column, in units of Ψ_0^2) and the phase (right column) of the droplet order parameter, in the lowest-energy state, for $N = 100$, $\omega = 0.05$, and $L/N = 0.0, 0.6, 1.0$, and 3.0 , respectively. The unit of length is x_0 . (e) Solid line, with data points: The corresponding dispersion relation in the rotating frame, i.e., $E_{\text{rot}}(L/N) - E(L/N = 0)$ as function of L/N , with $\Omega = 0.051$. Dashed line: Same as above for the center-of-mass excitation of the nonrotating state. The unit of energy is E_0 and the unit of angular momentum is \hbar .

that we reached the lowest-energy state for each value of

the angular momentum.

In what follows below we present the results for four different values of N , for $N = 50$ (droplets of “small” size), $N = 100$ and $N = 200$ (droplets of “intermediate” size), and $N = 270$ (droplets of “larger” size). These values of N were chosen as representative in the sense that they give the more general picture of this problem, which has a rather rich structure.

B. Rotational properties of droplets of “small” size

Varying L/N between 0 and 110 we show in Fig. 1 the result of such a calculation, for the density and the phase of the order parameter, as well as for the energy $E(L)$, with $\omega = 0.05$ and $N = 50$, i.e., $N\omega = 2.5$. Fitting the energy with a quadratic polynomial, we find that

$$E(L) \approx -10.6375 + 0.050002 L + 6.378 \times 10^{-8} L^2. \quad (5)$$

Both from the density [Figs. 1(a) and 1(b)], as well as from the dispersion relation [Fig. 1(c)], it is clear that we have center-of-mass excitation of the droplet for these values of ω and N . The constant term -10.6375 in Eq. (5) is the energy of the nonrotating state. Equation (4) gives a total energy which is ≈ -15.1633 . This, combined with the zero-point energy of the harmonic potential in two dimensions, i.e., $N\omega$, gives -12.6633 . This number deviates from the numerical result -10.6375 and is lower due to the fact that for $N = 50$ the system has not yet reached the Thomas-Fermi limit and the (neglected) kinetic energy is not negligible. Turning to the term which is linear in L in Eq. (5), this is due to the harmonic potential, while the term which is quadratic in L is negligible. In other words, the more general result for $E(L)$ is, in this regime,

$$E(L) = E_{\text{COM}}(L) = E(L=0) + L\omega. \quad (6)$$

We stress that Eq. (6) provides an upper bound for the energy, for any value of N and L , as we explain in more detail below.

C. Rotational properties of droplets of “intermediate” size

For fixed ω and larger values of N the size of the droplet becomes comparable with a_{osc} , $\rho_0 \approx a_{\text{osc}}$. In this case the droplet starts to get “squeezed” due to the trapping potential. Thus, the trapping potential tends to increase the mean value of the density of the droplet, \bar{n} . This, in turn, increases the energy due to the nonlinear term, too [see Eq. (4)]. In the presence of a vortex state \bar{n} drops and therefore a vortex state may be energetically favorable. Indeed, as we have also seen numerically, as N , or as ω , increase, we have vortex, rather than center-of-mass excitation of the droplet.

Such an example is shown in Fig. 2, where $N = 100$ and $\omega = 0.05$, i.e., $N\omega = 5$. Here we see that for small values of L the axial symmetry of the droplet is distorted

[Fig. 2(b)]. This is due to the fact that two vortices approach the droplet from opposite sides, with one being further away from the trap center than the other. Eventually, when $L = N$ the vortex state that is closer moves to the center of the trap and the density of the droplet becomes axially symmetric [Fig. 2(c)]. For even larger values of L , $L > N$, however, instead of more vortices entering the cloud, the extra angular momentum is carried via center-of-mass excitation of the state with $L = N$, i.e., the state with one vortex located at the center of the droplet, as shown in Fig. 2(d). This is in sharp contrast with the case of contact interactions. It is a generic result and is one of the novel aspects of the present study.

The corresponding dispersion relation is also shown in Fig. 2(e). Instead of plotting it in the laboratory frame, we choose to plot it in the rotating frame (in this plot and in all the other plots of the dispersion relation that follow below), because its structure is more clearly visible. More specifically, we plot $E_{\text{rot}}(L/N) - E(L/N=0)$, where $E_{\text{rot}}(L/N) = E(L/N) - L\Omega$, with $\Omega = 0.051$ (i.e., we choose a slightly larger value of Ω than $\omega = 0.05$). When $L > N$, we see that the dispersion relation becomes linear, as expected, since the nonlinear term of the energy is unaffected by the angular momentum in this range of L (simply because the shape of the droplet does not depend on L in this range of L).

To get a more quantitative description of the transition from center-of-mass to vortex excitation, let us consider the eigenfunctions $\phi_m(\rho, \theta)$ of the two lowest-Landau levels as trial order parameters for the ground, nonrotating state (where $L = 0$), assuming that the oscillator length a_{osc} is equal to ρ_0 ,

$$\phi_0 = \frac{\sqrt{N}}{\sqrt{\pi\rho_0}} e^{-\rho^2/(2\rho_0^2)}, \quad (7)$$

and for the state with one singly quantized vortex (where $L = N$),

$$\phi_1 = \frac{\sqrt{N}}{\sqrt{\pi\rho_0^2}} \rho e^{i\theta} e^{-\rho^2/(2\rho_0^2)}. \quad (8)$$

Evaluating the energy due to the nonlinear term,

$$E_{\text{int},i} = \frac{1}{2} \int |\phi_i|^4 \ln \frac{|\phi_i|^2}{\sqrt{e}} d^2\rho. \quad (9)$$

For the state ϕ_0 we find

$$\frac{E_{\text{int},0}}{N} = \frac{N}{4\pi\rho_0^2} \left(\ln \frac{N}{\pi\sqrt{e}\rho_0^2} - \frac{1}{2} \right) = \frac{\bar{n}}{4} \left(\ln \frac{\bar{n}}{\sqrt{e}} - \frac{1}{2} \right),$$

while for the state ϕ_1 ,

$$\begin{aligned} \frac{E_{\text{int},1}}{N} &\approx \frac{N}{2\pi\rho_0^2} \left(\frac{1}{4} \ln \frac{N}{\pi\sqrt{e}\rho_0^2} - \frac{3}{8} + 0.057 \right) \\ &= \frac{\bar{n}}{2} \left(\frac{1}{4} \ln \frac{\bar{n}}{\sqrt{e}} - \frac{3}{8} + 0.057 \right). \end{aligned} \quad (10)$$

When we have center-of-mass excitation (of the state with $L = 0$), from Eq. (6) it follows that

$$E_{\text{COM}}(L=N) - E(L=0) = N\omega. \quad (11)$$

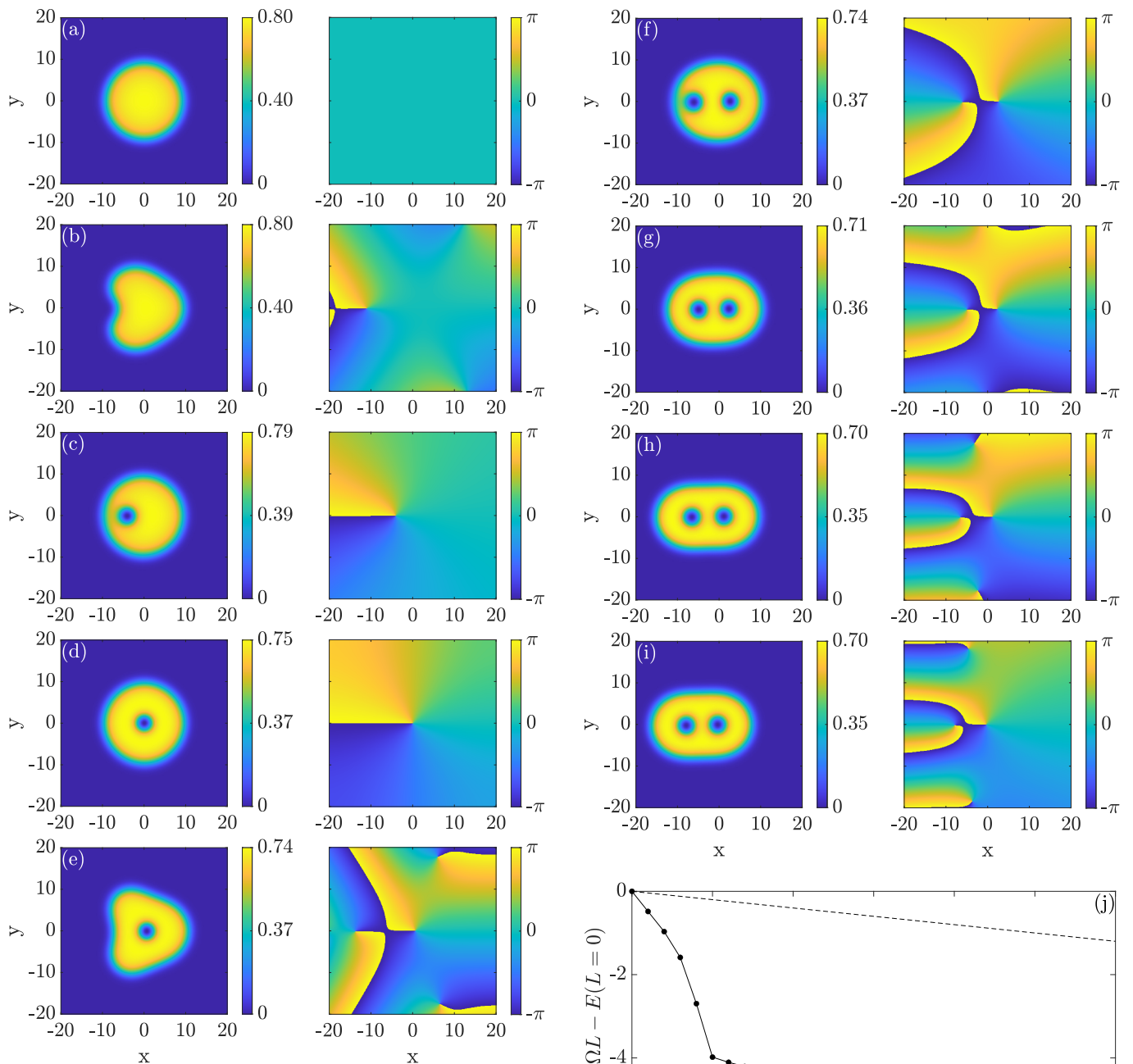


FIG. 3: [(a)–(e)] The density (left column, in units of Ψ_0^2) and the phase (right column) of the droplet order parameter, in the lowest-energy state, for $N = 200$, $\omega = 0.05$, and $L/N = 0.0, 0.2, 0.8, 1.0$, and 1.2 , respectively. The unit of length is x_0 .

When we have vortex excitation,

$$E_{\text{vor}}(L = N) - E(L = 0) = N\omega + E_{\text{int},1} - E_{\text{int},0}. \quad (12)$$

From the last two equations, we see that it is the difference $E_{\text{int},1} - E_{\text{int},0}$ which determines whether we will have center-of-mass, or vortex excitation. It turns out that the critical value of N/ρ_0^2 which gives $E_{\text{int},1} = E_{\text{int},0}$ is approximately equal to 4. If $\rho_0^2 = a_{\text{osc}}^2 = 1/\omega = 20$, then the critical value of N is approximately 80. We stress that the calculation presented above compares the energy between the ground state and the state with one

FIG. 3: (Cont.) [(f)–(i)] Same as panels [(a)–(e)] except for $L/N = 1.6, 2.0, 2.6$, and 3.0 , respectively. (j) Solid line, with data points: the corresponding dispersion relation in the rotating frame, i.e., $E_{\text{rot}}(L/N) - E(L/N = 0)$ as a function of L/N , with $\Omega = 0.051$. Dashed line: same as above for the center-of-mass excitation of the nonrotating state. The unit of energy is E_0 and the unit of angular momentum is \hbar .

vortex located at the center of the droplet. From our numerical results it follows that, for $\omega = 0.05$, the critical number of N for the transition from center-of-mass excitation to vortex excitation is between 98.6 and 98.7.

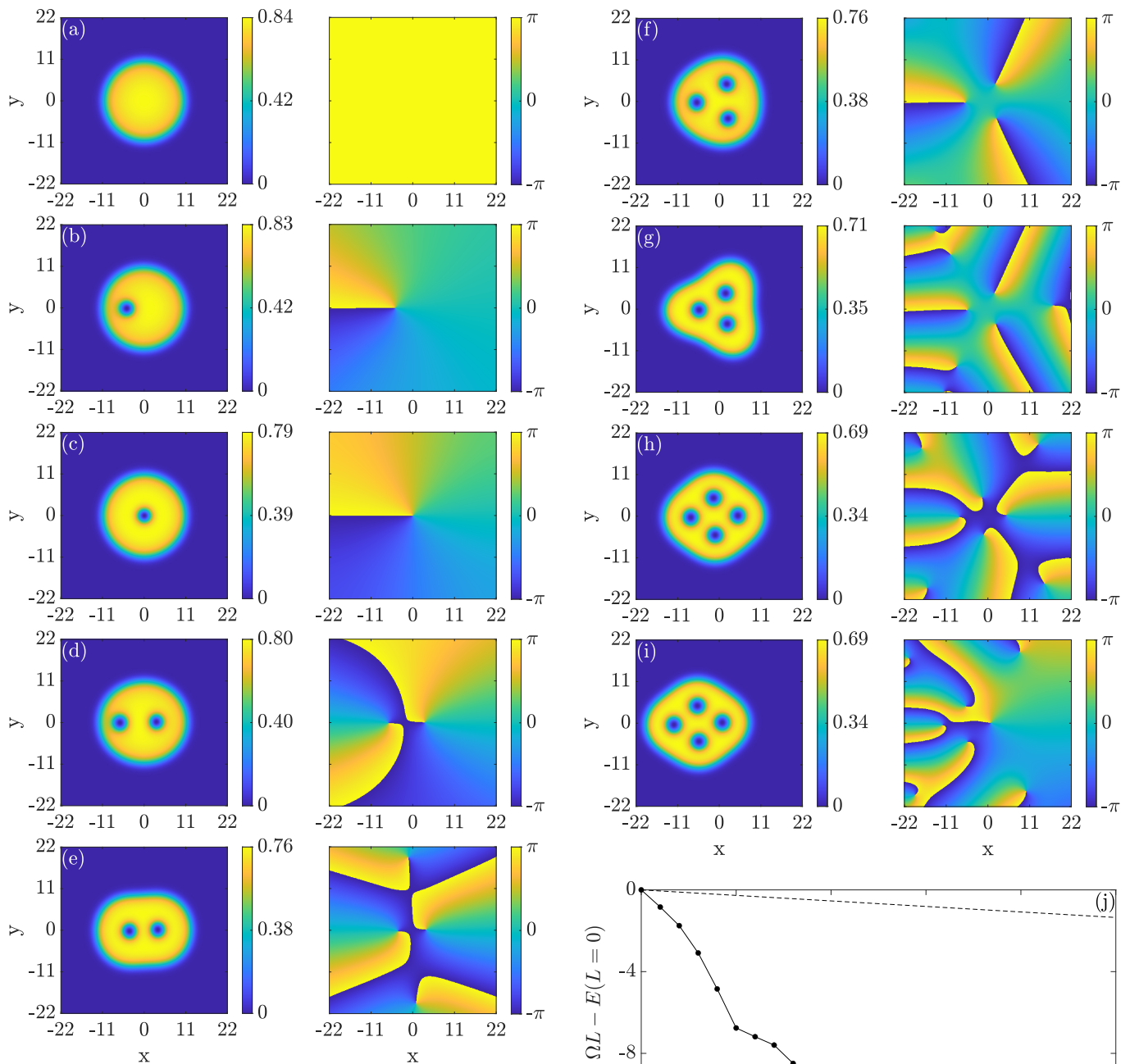


FIG. 4: [(a)–(e)] The density (left column, in units of Ψ_0^2) and the phase (right column) of the droplet order parameter, in the lowest-energy state, for $N = 270$, $\omega = 0.05$, and $L/N = 0.0, 0.8, 1.0, 1.6$, and 2.0 , respectively. The unit of length is x_0 .

To examine what happens for even larger values of N , we show in Fig. 3 the result of our calculations for $N = 200$ and $\omega = 0.05$, i.e., $N\omega = 10$. We observe that for $0 < L < N$ the droplet is again distorted from axial symmetry due to the approach of a vortex from infinity [Figs. 3(b) and 3(c)]. When $L = N$ this vortex ends up again at the center of the droplet [Fig. 3(d)]. However, here that the atom number N is larger, for $L > N$ a second vortex enters the system, and eventually a twofold symmetric state forms [Figs. 3(e) to 3(g)]. Here it is only for L/N larger than ≈ 2.6 that the droplet carries its additional

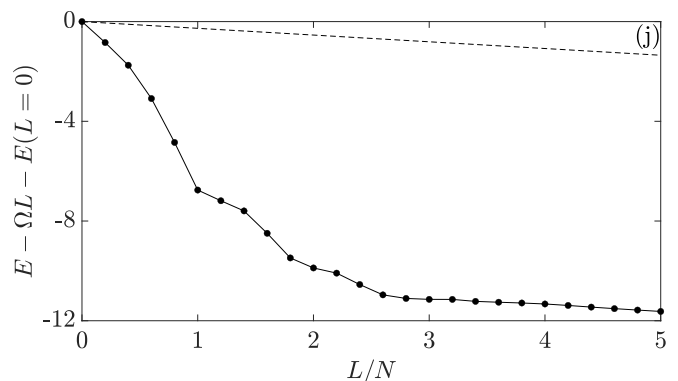


FIG. 4: (Cont.) [(f)–(i)] Same as panels [(a)–(e)] except for $L/N = 2.4, 3.0, 3.4$, and 5.0 , respectively. The unit of length is x_0 . (j) Solid line, with data points: the corresponding dispersion relation in the rotating frame, i.e., $E_{\text{rot}}(L/N) - E(L/N = 0)$ as a function of L/N , with $\Omega = 0.051$. Dashed line: same as above for the center-of-mass excitation of the nonrotating state. The unit of energy is E_0 and the unit of angular momentum is \hbar .

angular momentum via center-of-mass excitation, i.e., via a “mixed” state, as shown in Figs. 3(h) and 3(i). The dispersion relation (in the rotating frame), which is also

shown in Fig. 3(j), becomes linear again, now for L/N exceeding ≈ 2.6 .

D. Rotational properties of droplets of “larger” size

In Fig. 4 we have considered an even larger value of $N = 270$, with ω still being equal to 0.05 ($N\omega = 13.5$). Clearly the mean density of the nonrotating droplet also increases. As a result, we observe up to four vortices which are energetically favorable [Figs. 4(a) to 4(h)], before the “mixed” state, i.e., the center-of-mass excitation of this state with four vortices, becomes the state of lowest energy, for L/N exceeding ≈ 3.4 [Fig. 4(i)]. As in the case of droplets of “intermediate” size, the dispersion relation, which is shown in Fig. 4(j), becomes linear beyond this L/N value.

E. Fixing Ω instead of L

Up to now all our results have been derived for fixed L . From the dispersion relation, one may also evaluate the angular momentum of the droplet if Ω is fixed, instead. More specifically, having evaluated the dispersion relation (i.e., the lowest energy $E(L)$ as function of L), we consider the energy in the rotating frame $E_{\text{rot}}(L) = E(L) - L\Omega$. For some fixed Ω we find the value of L that minimizes $E_{\text{rot}}(L)$ and that is how $L/N(\Omega)$, i.e., Fig. 5, is produced.

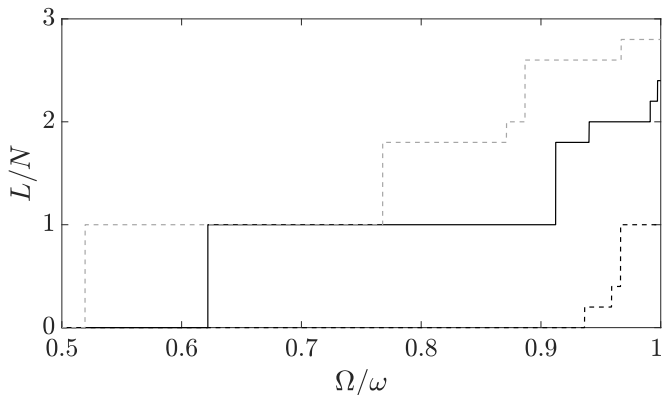


FIG. 5: The functions $L/N = L/N(\Omega/\omega)$, derived from the lowest-energy states, for $N = 100$ (black, dashed curve), 200 (black, solid curve), and 270 (gray, dashed curve), with $\omega = 0.05$. The unit of angular momentum is \hbar .

Figure 5 shows $L/N = L/N(\Omega/\omega)$, for $N = 100, 200$, and 270, with $\omega = 0.05$ (the steps in the angular momentum per particle L/N that we used to produce this plot were equal to 0.2). In this plot we see the usual plateaus, also known in the case of single-component condensates with an effectively repulsive contact interaction. We stress that for $\Omega \rightarrow \omega^-$, this plot diverges, as we argue in the following section [see Eq. (16) and the relevant discussion].

IV. GENERAL PICTURE AND LIMIT OF RAPID ROTATION

From the examples presented above, and other cases that we have investigated, one may get the more general picture that emerges in this system. For sufficiently small N (when $\rho_0 \ll a_{\text{osc}}$) we have center-of-mass excitation of the nonrotating ground state for all values of L . For larger values of N , where $\rho_0 \gtrsim a_{\text{osc}}$, with increasing L one, or more vortices enter the cloud. However, there is a limit to this. As the number of vortices increases, \bar{n} drops. Decreasing \bar{n} even further, is not energetically favorable. As a result, if L increases further, the additional angular momentum is carried via center-of-mass excitation of some “mixed” state. The dispersion relation also becomes a straight line beyond this specific value of L .

One estimate for the maximum number of vortices N_v that the droplet accommodates before it turns to center-of-mass excitation is that the mean density is equal to the one that minimizes the energy of Eq. (4), i.e., $\bar{n} = 1/\sqrt{e}$,

$$\frac{N}{S - N_v \sigma} = \frac{1}{\sqrt{e}}. \quad (13)$$

Here S and σ are the “surfaces” of the droplet and of each vortex, respectively. An approximate expression for σ is $\sigma \approx \pi \xi^2$, where the coherence length ξ gives roughly the linear size of the vortex.

According to the analysis presented above, one may also make a general statement about the dispersion relation. For any two states with angular momentum L_1 and L_2 , with $L_1 < L_2$, $E(L_2)$ has to be lower than $E(L_1) + (L_2 - L_1)\omega$,

$$E(L_2) < E(L_1) + (L_2 - L_1)\omega. \quad (14)$$

If this inequality is violated, one may always start with the state of angular momentum L_1 and excite it via center-of-mass excitation to a state with angular momentum L_2 . In this case, $E(L_2)$ will be equal to $E(L_1) + (L_2 - L_1)\omega$. From Eq. (14) it also follows that, for $L_2 \rightarrow L_1$,

$$\frac{dE(L)}{dL} < \omega, \quad (15)$$

i.e., the slope of the dispersion relation cannot exceed ω .

Another consequence of Eq. (14) is that, if one works with a fixed rotational frequency of the trap Ω and not with a fixed angular momentum, Ω cannot exceed ω . Indeed, according to Eq. (14),

$$E_{\text{rot}}(L_2) < E_{\text{rot}}(L_1) + (L_2 - L_1)(\omega - \Omega). \quad (16)$$

Therefore, if $\Omega \geq \omega$, $E_{\text{rot}}(L_2) < E_{\text{rot}}(L_1)$ and $E_{\text{rot}}(L)$ is a decreasing function of L . In other words, if Ω exceeds ω , then the energy is unbounded. This result is a combined effect of the “mixed” state that we have seen, with the centrifugal force, which gives rise to the effective potential $M(\omega^2 - \Omega^2)\rho^2/2$. Last but not least, we stress that this result is also true in the case of contact interactions, in a harmonic trapping potential.

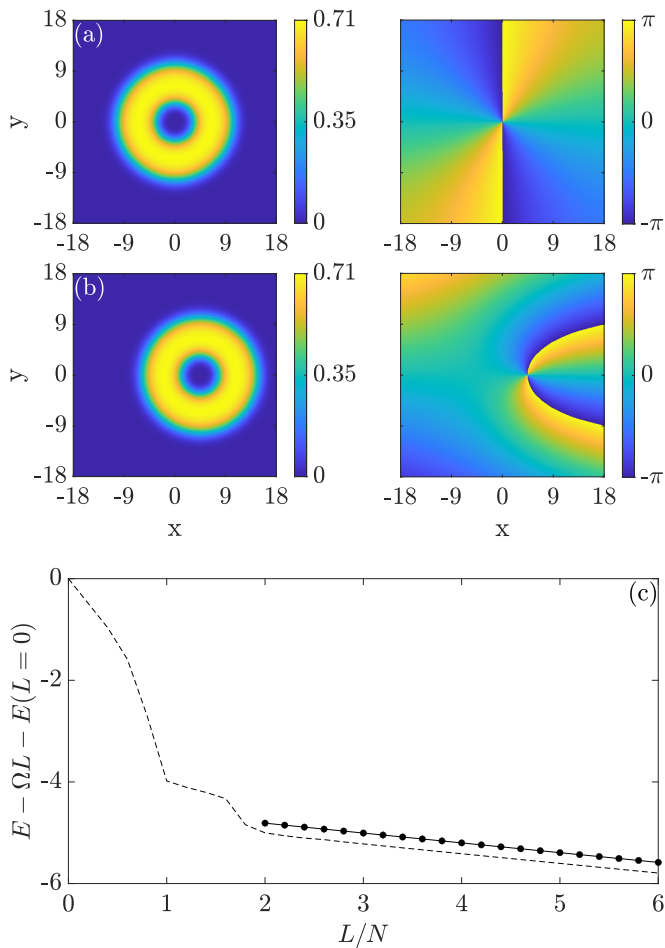


FIG. 6: [(a), (b)] The density (left column, in units of Ψ_0^2) and the phase (right column) of the droplet order parameter, in the excited, multiply quantized vortex state(s) $\Psi_{S=2}$, for $N = 200$, $\omega = 0.05$, and $L/N = 2.0$ and 3.0 , respectively. The unit of length is x_0 . (c) Solid line, with data points: the corresponding dispersion relation in the rotating frame, i.e., $E_{\text{rot}}(L/N) - E(L/N = 0)$ as a function of L/N , with $\Omega = 0.051$. Dashed line: same as above for the lowest-energy state. The unit of energy is E_0 and the unit of angular momentum is \hbar .

V. EXCITATION SPECTRUM

All the states that we have presented so far are those of lowest energy, for a fixed N and L . Although this is one of the most important questions, a separate question is the excitation spectrum. We should stress that the excitation spectrum is not only interesting theoretically, but is also experimentally relevant. While we have not made a complete study of the excited states, we have managed to find at least part of them. Interestingly enough, the arguments presented in Sec. IV allow us to get a rather easy understanding of this problem and to even predict the existence of the states that we have identified.

In the results which are presented below, we have focused on the case $N = 200$ and $\omega = 0.05$ and we have identified two classes of states in the excitation spectrum. The first class includes multiply quantized vortex states,

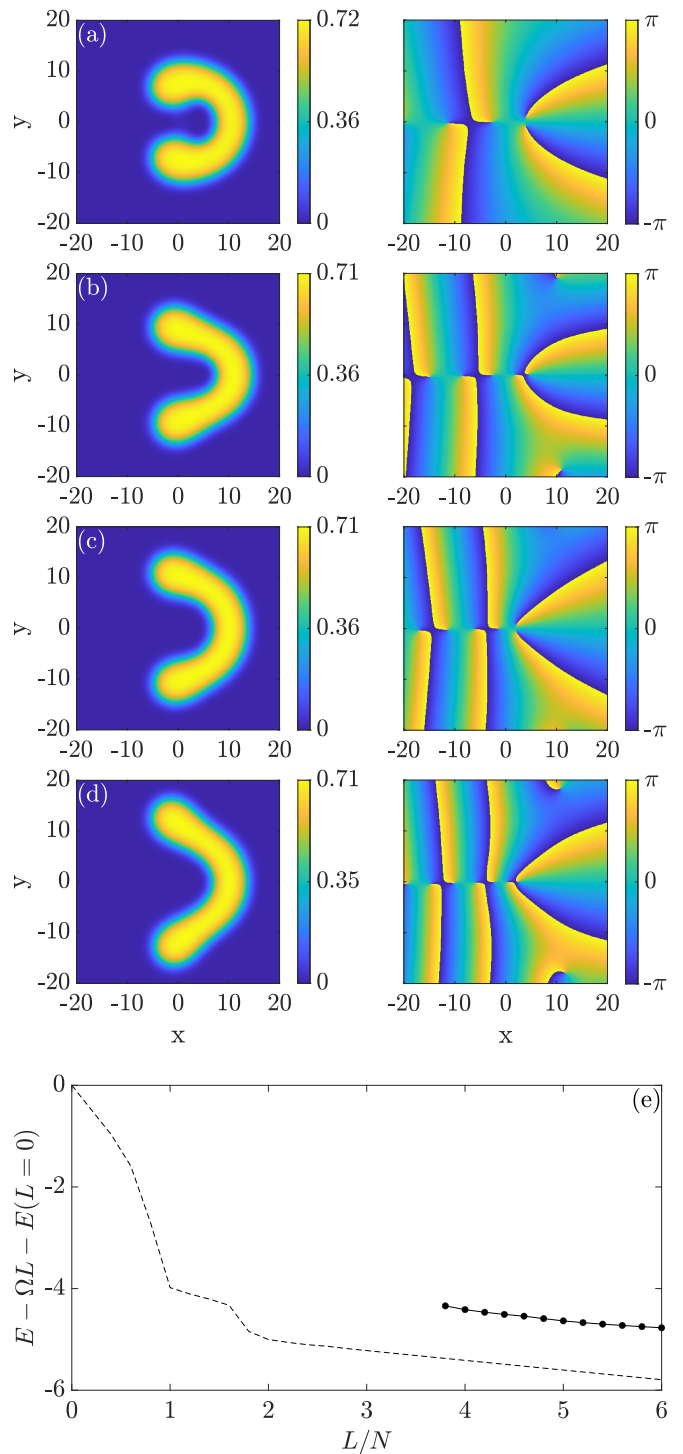


FIG. 7: [(a)–(d)] The density (left column, in units of Ψ_0^2) and the phase (right column) of the droplet order parameter, in the excited states with an axially asymmetric density distribution for $N = 200$, $\omega = 0.05$, and $L/N = 3.8, 4.4, 5.0$, and 5.6 , respectively. The unit of length is x_0 . (e) Solid line, with data points: the corresponding dispersion relation in the rotating frame, i.e., $E_{\text{rot}}(L/N) - E(L/N = 0)$ as function of L/N , with $\Omega = 0.051$. Dashed line: same as above for the lowest-energy state. The unit of energy is E_0 and the unit of angular momentum is \hbar .

of the form $\Psi_S(\rho, \theta) = f(\rho)e^{iS\theta}$, where S is the winding

number, which have an axially symmetric density distribution. These are solutions of the equation

$$-\frac{1}{2}\frac{\partial^2 f}{\partial \rho^2} - \frac{1}{2\rho}\frac{\partial f}{\partial \rho} + \frac{S^2}{2\rho^2}f + \frac{1}{2}\omega^2\rho^2f + |f|^2 \ln |f|^2 f = \mu f. \quad (17)$$

Starting with $L/N = S = 2$, we have found that this doubly quantized vortex state [Fig. 6(a)], $\Psi_{S=2}$, is very close in energy with the actual state of lowest energy, as shown in Fig. 6(c). This proximity is not a surprise, but rather is expected, i.e., it is due to the fact that the mean densities of the two states are very close to each other. For $L/N > 2$, we then have center-of-mass excitation of the doubly quantized vortex state [Fig. 6(b)], with an energy which increases linearly with the angular momentum, as we saw earlier. Clearly what we described for $L/N \geq 2$ is general. For example, the state $\Psi_{S=3}$ is also present in the excitation spectrum for all values of $L/N \geq 3$, etc.

The multiply quantized vortex states described above have an axially symmetric density distribution with respect to their center of mass. The second class of states that we have identified in the excitation spectrum, are states which break the axial symmetry of the problem. In this case the centrifugal term [i.e., the third term on the left in Eq. (17)] favors an axially asymmetric density distribution. As a result, the cloud “localizes”, since this is energetically more favorable (in order, again, for the droplet to achieve the optimal mean density). Examples of such excited states are shown in Figs. 7(a) to 7(d), as well as the corresponding energy in Fig. 7(e).

VI. PHYSICAL UNITS AND EXPERIMENTAL RELEVANCE OF OUR RESULTS

As mentioned above, up to now we have used dimensionless units. Here we show how one may return to the physical units and then we give some estimates for the experimentally relevant scales.

First of all, let us denote as Ψ_\uparrow and Ψ_\downarrow the order parameter of each component. In the symmetric case that we consider in the present problem, $\Psi_\uparrow = \Psi_\downarrow$ and also $\int |\Psi_\uparrow|^2 d^2\rho = \int |\Psi_\downarrow|^2 d^2\rho = N/2$, where N is the total number of atoms in both components. Let us also introduce $\Psi = \sqrt{2}\Psi_\uparrow = \sqrt{2}\Psi_\downarrow$, where obviously $\int |\Psi|^2 d^2\rho = N$.

The order parameter Ψ satisfies the equation

$$i\hbar\frac{\partial\Psi}{\partial t} = -\frac{\hbar^2}{2M}\nabla^2\Psi + \frac{1}{2}M\omega^2\rho^2\Psi + \frac{4\pi\hbar^2}{M\ln^2(a_{\uparrow\downarrow}/a)}|\Psi|^2\ln\frac{|\Psi|^2}{2\sqrt{e}n_0}\Psi. \quad (18)$$

Here M is the atom mass, which is assumed to be the same for the two components and ω is the frequency of the (two-dimensional) trapping potential. Also, a and $a_{\uparrow\downarrow}$ are the two-dimensional scattering lengths for elastic atom-atom collisions between the same species (assumed to be equal for the two components) and for different

species, respectively. Furthermore,

$$n_0 = \frac{e^{-2\gamma-3/2}\ln(a_{\uparrow\downarrow}/a)}{2\pi aa_{\uparrow\downarrow}}. \quad (19)$$

Here γ is Euler’s constant, $\gamma \approx 0.5772$, while

$$\ln(a_{\uparrow\downarrow}/a) = \sqrt{\frac{\pi}{2}}\left(\frac{a_z}{a^{3D}} - \frac{a_z}{a_{\uparrow\downarrow}^{3D}}\right). \quad (20)$$

Here a_z is the “width” of the droplet along the axis of rotation, and a^{3D} , $a_{\uparrow\downarrow}^{3D}$ are the three-dimensional scattering lengths for elastic atom-atom collisions between the same and different species, respectively. Introducing

$$\Psi_0^2 = 2\sqrt{e}n_0 = \frac{e^{-2\gamma-1}\ln(a_{\uparrow\downarrow}/a)}{\pi aa_{\uparrow\downarrow}} \quad (21)$$

and setting $\tilde{\Psi} = \Psi/\Psi_0$, Eq. (18) becomes

$$i\frac{\partial\tilde{\Psi}}{\partial\tilde{t}} = -\frac{1}{2}\tilde{\nabla}^2\tilde{\Psi} + \frac{1}{2}\tilde{\omega}^2\tilde{\rho}^2\tilde{\Psi} + |\tilde{\Psi}|^2\ln|\tilde{\Psi}|^2\tilde{\Psi}. \quad (22)$$

Here $\tilde{t} = t/t_0$, where

$$t_0 = \frac{Maa_{\uparrow\downarrow}\ln(a_{\uparrow\downarrow}/a)}{4\hbar e^{-2\gamma-1}}. \quad (23)$$

Also, $\tilde{\rho} = \rho/x_0$ and $\tilde{\nabla}^2$ is the dimensionless Laplacian, with the unit of length being x_0 , where

$$x_0 = \sqrt{\frac{aa_{\uparrow\downarrow}\ln(a_{\uparrow\downarrow}/a)}{4e^{-2\gamma-1}}}. \quad (24)$$

Furthermore, $\tilde{\omega} = \omega/\omega_0$, where the units of the frequency ω_0 and of the energy E_0 , are

$$E_0 = \hbar\omega_0 = \frac{\hbar}{t_0} = \frac{\hbar^2}{Mx_0^2} = \frac{\hbar^2}{Maa_{\uparrow\downarrow}\ln(a_{\uparrow\downarrow}/a)}. \quad (25)$$

The normalization condition takes the form

$$\int |\tilde{\Psi}|^2 d^2\tilde{\rho} = \frac{N}{N_0}, \quad (26)$$

where

$$N_0 = \Psi_0^2 x_0^2 = \frac{1}{4\pi}\ln^2(a_{\uparrow\downarrow}/a), \quad (27)$$

which is the unit of N .

Finally, the time-independent equation that corresponds to Eq. (22) is derived after we set $\Psi(\tilde{\rho}, \tilde{t}) = \Psi(\tilde{\rho})e^{-i\tilde{\mu}\tilde{t}}$, where $\tilde{\mu}$ is the dimensionless chemical potential, thus getting

$$-\frac{1}{2}\tilde{\nabla}^2\tilde{\Psi} + \frac{1}{2}\tilde{\omega}^2\tilde{\rho}^2\tilde{\Psi} + |\tilde{\Psi}|^2\ln|\tilde{\Psi}|^2\tilde{\Psi} = \tilde{\mu}\tilde{\Psi}. \quad (28)$$

We stress that the “tilde” used in the symbols in the present section, which represents dimensionless quantities, is dropped in all the other sections for convenience.

Equation (27) allows us to evaluate the actual (total) number of atoms in a droplet. For a typical value of

$a_z = 0.1 \mu\text{m}$ and $a^{3\text{D}} = 10.1 \text{ nm}$, $a_{\uparrow\downarrow}^{3\text{D}} = -10.0 \text{ nm}$, $\ln(a_{\uparrow\downarrow}/a) \approx 25$. Then, according to Eq. (27), $N_0 \approx 50$. Therefore, the range of N that we have considered (50 up to 270) corresponds roughly to ≈ 2500 , up to ≈ 14000 atoms in an experiment.

Also, the unit of length x_0 turns out to be on the order of $1 \mu\text{m}$. This implies that, for e.g., 10^4 atoms, the size of a (nonrotating) droplet in the Thomas-Fermi limit, which was evaluated in Sec. III, is $\approx 10 \mu\text{m}$. Finally, typical values of the two-dimensional density are $\approx 10^9 \text{ cm}^{-2}$, of the three-dimensional density are 10^{13} cm^{-3} , t_0 is on the order of millisecond and the typical value of the trapping potential is hundreds of hertz.

VII. SUMMARY OF THE RESULTS WITH A COMPARISON WITH THE PROBLEM OF CONTACT INTERACTIONS

In the present study we investigated the rotational behavior of a quasi-two-dimensional quantum droplet, which consists of a mixture of two distinguishable Bose-Einstein condensed gases, assuming that the droplet is confined in a harmonic trapping potential.

For a fixed trap frequency and sufficiently small atom numbers, the droplet does not host any vortices, but rather it carries its angular momentum via center-of-mass excitation of its nonrotating, ground state. This is very much like the case of a single-component Bose-Einstein condensed gas, which has an effectively attractive interatomic interaction potential and is confined in a harmonic trap. The only difference between the two problems is that, while in the case of droplets we have a stable system (as a consequence of quantum fluctuations), in the case of a single component the system is metastable.

For a larger atom number, and sufficiently small values of the angular momentum, the droplet behaves in the usual way, with vortices entering it as the angular momentum increases. As more and more vortices enter the droplet, its average density drops, which is energetically favorable. However, as the number of vortices increases, eventually it is no longer energetically favorable for even more vortices to enter the droplet. As a result, beyond some critical value of the angular momentum the droplet

carries the additional angular momentum via center-of-mass excitation of a vortex-carrying state.

For a single-component, harmonically trapped Bose-Einstein condensate with an effectively attractive interaction the angular momentum is carried via center-of-mass excitation of the nonrotating state, for all values of the angular momentum. On the contrary, for an effectively repulsive interaction this never happens (in the lowest-energy state) [51]. Furthermore, for a contact potential with an effective repulsive interaction, the interaction energy is a decreasing function of the density.

In the case of a two-component system, i.e., in quantum droplets, the situation is different due to a simple and important difference between the two problems. Here, the interaction energy is not a monotonic function of the density [see Eq. (4)], but rather it has a minimum at some specific value of the density.

As a result, as L increases, in the case of a contact potential with an effective repulsive interaction, the cloud expands radially and this lowers its mean density and the corresponding interaction energy. Eventually, the system enters the highly correlated ‘‘Laughlin-like’’ regime that we mentioned in the Introduction. On the other hand, for the case of droplets (i.e., two-component systems), the decrease of the mean density due to the vortices—for a sufficiently large atom number—is energetically favorable only until the density reaches some finite value.

The important conclusion that follows from the above discussion is the following: For increasing L , in a single-component condensate the gas enters the highly correlated Laughlin regime. On the other hand, when we have two components, i.e., in the case of droplets, for a sufficiently large angular momentum, a droplet is always in a ‘‘mixed’’ state, i.e., in a state of center-of-mass excitation of a state which includes vortices.

Our study demonstrates the richness of this problem, in terms of the various physical states. In addition, it also demonstrates that, despite the difference of the phases that we have found, there is a universal behavior of the droplets in the limit of rapid rotation, in a ‘‘mixed’’ state, which has never been seen before in any other ‘‘traditional’’ superfluid, including liquid helium and harmonically trapped condensed atoms interacting with contact interactions.

-
- [1] I. Bloch, J. Dalibard, and W. Zwerger, *Rev. Mod. Phys.* **80**, 885 (2008).
 - [2] S. Viefers, *J. Phys. Cond. Mat.* **20**, 123202 (2008).
 - [3] N. R. Cooper, *Advances in Physics* **57**, 539 (2008).
 - [4] A. L. Fetter, *Rev. Mod. Phys.* **81**, 647 (2009).
 - [5] H. Saarikoski, S. M. Reimann, A. Harju, and M. Manninen, *Rev. Mod. Phys.* **82**, 2785 (2010).
 - [6] D. S. Petrov, *Phys. Rev. Lett.* **115**, 155302 (2015).
 - [7] F. Böttcher, J.-N. Schmidt, J. Hertkorn, K. S. H. Ng, S. D. Graham, M. Guo, T. Langen, and T. Pfau, *Reports on Progress in Physics* **84**, 012403 (2021).
 - [8] Z.-H. Luo, W. Pang, B. Liu, Y.-Y. Li, and B. A. Malomed, *Frontiers of Physics* **16**, 32201 (2021).
 - [9] D. S. Petrov and G. E. Astrakharchik, *Phys. Rev. Lett.* **117**, 100401 (2016).
 - [10] Yongyao Li, Zhihuan Luo, Yan Liu, Zhaopin Chen, Chunqing Huang, Shenhe Fu, Haishu Tan, and Boris A. Malomed, *New J. Phys.* **19**, 113043 (2017).
 - [11] G. E. Astrakharchik and B. A. Malomed, *Phys. Rev. A* **98**, 013631 (2018).
 - [12] Y. V. Kartashov, B. A. Malomed, L. Tarruell, and L. Torner, *Phys. Rev. A* **98**, 013612 (2018).
 - [13] A. Cidrim, F. E. A. dos Santos, E. A. L. Henn, and T. Macrı, *Phys. Rev. A* **98**, 023618 (2018).
 - [14] Paweł Zin, Maciej Pylak, Tomasz Wasak, Mariusz Gajda, and Zbigniew Idziaszek, *Phys. Rev. A* **98**, 051603(R) (2018).

- (2018).
- [15] F. Ancilotto, M. Barranco, M. Guilleumas, and M. Pi, *Phys. Rev. A* **98**, 053623 (2018).
- [16] Y. Li, Z. Chen, Z. Luo, C. Huang, H. Tan, W. Pang, and B. A. Malomed, *Phys. Rev. A* **98**, 063602 (2018).
- [17] L. Parisi, G. E. Astrakharchik, and S. Giorgini, *Phys. Rev. Lett.* **122**, 105302 (2019).
- [18] Y. V. Kartashov, B. A. Malomed, and L. Torner, *Phys. Rev. Lett.* **122**, 193902 (2019).
- [19] Xiliang Zhang, Xiaoxi Xu, Yiyin Zheng, Zhaopin Chen, Bin Liu, Chunqing Huang, Boris A. Malomed, and Yongyao Li, *Phys. Rev. Lett.* **123**, 133901 (2019).
- [20] M. Nilsson Tengstrand, P. Stürmer, E. Ö. Karabulut, and S. M. Reimann, *Phys. Rev. Lett.* **123**, 160405 (2019).
- [21] Bin Liu, Hua-Feng Zhang, Rong-Xuan Zhong, Xi-Liang Zhang, Xi-Zhou Qin, Chunqing Huang, Yong-Yao Li, and Boris A. Malomed, *Phys. Rev. A* **99**, 053602 (2019).
- [22] R. Tamil Thiruvalluvar, S. Sabari, K. Porsezian, P. Murganandam, *Physica E* **107**, 54 (2019).
- [23] G. Ferioli, G. Semeghini, S. Terradas-Briansó, L. Masi, M. Fattori, and M. Modugno, e-print arXiv:1912.09594.
- [24] Ivan Morera, Grigori E. Astrakharchik, Artur Polls, and Bruno Juliá-Díaz, e-print arXiv:2001.04796.
- [25] Luca Parisi and Stephano Giorgini, e-print arXiv:2003.05231.
- [26] Marek Tylutki, Grigori E. Astrakharchik, Boris A. Malomed, and Dmitry S. Petrov, e-print arXiv:2003.05803.
- [27] P. Examilioti and G. M. Kavoulakis, *J. Phys. B: At. Mol. Opt. Phys.* **53**, 175301 (2020).
- [28] Liangwei Dong and Yaroslav V. Kartashov, *Phys. Rev. Lett.* **126**, 244101 (2021).
- [29] Yanming Hu, Yifan Fei, Xiao-Long Chen and Yunbo Zhang, *Frontiers of Physics* **17**, 61505 (2022).
- [30] Qi Gu and Xiaoling Cui, e-print arXiv:2306.14958.
- [31] T. A. Yoğurt, U. Tanyeri, A. Keleş, and M. Ö. Oktel, e-print arXiv:2308.02704.
- [32] T. A. Flynn, N. A. Keeper, N. G. Parker, and T. P. Billam, e-print arXiv:2309.04300.
- [33] Xucong Du, Yifan Fei, Xiao-Long Chen, and Yunbo Zhang, e-print arXiv:2309.05245.
- [34] Szu-Cheng Cheng, Yu-Wen Wang, and Wen-Hsuan Kuan, e-print arXiv:2302.07481.
- [35] C. Cabrera, L. Tanzi, J. Sanz, B. Naylor, P. Thomas, P. Cheiney, and L. Tarruell, *Science* **359**, 301 (2018).
- [36] P. Cheiney, C. R. Cabrera, J. Sanz, B. Naylor, L. Tanzi, and L. Tarruell, *Phys. Rev. Lett.* **120**, 135301 (2018).
- [37] G. Semeghini, G. Ferioli, L. Masi, C. Mazzinghi, L. Wolswijk, F. Minardi, M. Modugno, G. Modugno, M. Inguscio, and M. Fattori, *Phys. Rev. Lett.* **120**, 235301 (2018).
- [38] Giovanni Ferioli, Giulia Semeghini, Leonardo Masi, Giovanni Giusti, Giovanni Modugno, Massimo Inguscio, Albert Gallemí, Alessio Recati, and Marco Fattori, *Phys. Rev. Lett.* **122**, 090401 (2019).
- [39] C. D’Errico, A. Burchianti, M. Prevedelli, L. Salasnich, F. Ancilotto, M. Modugno, F. Minardi, and C. Fort, *Phys. Rev. Research* **1**, 033155 (2019).
- [40] H. Kadau, M. Schmitt, M. Wenzel, C. Wink, T. Maier, I. Ferrier-Barbut, and T. Pfau, *Nature* **530**, 194 (2016).
- [41] M. Schmitt, M. Wenzel, F. Böttcher, I. Ferrier-Barbut, and T. Pfau, *Nature* **539**, 259 (2016).
- [42] I. Ferrier-Barbut, H. Kadau, M. Schmitt, M. Wenzel, and T. Pfau, *Phys. Rev. Lett.* **116**, 215301 (2016).
- [43] I. Ferrier-Barbut, M. Schmitt, M. Wenzel, H. Kadau, and T. Pfau, *J. Phys. B* **49**, 214004 (2016).
- [44] I. Ferrier-Barbut, M. Wenzel, F. Böttcher, T. Langen, M. Isoard, S. Stringari, and T. Pfau, *Phys. Rev. Lett.* **120**, 160402 (2018).
- [45] L. Chomaz, S. Baier, D. Petter, M. J. Mark, F. Wächtler, L. Santos, and F. Ferlaino, *Phys. Rev. X* **6**, 041039 (2016).
- [46] T. D. Lee, K. Huang, and C. N. Yang, *Phys. Rev.* **106**, 1135 (1957).
- [47] M. Gulliksson and M. Ögren, *J. Phys. A: Math. Theor.* **54**, 275304 (2021).
- [48] N. K. Wilkin, J. M. F. Gunn, and R. A. Smith, *Phys. Rev. Lett.* **80**, 2265 (1998).
- [49] B. Mottelson, *Phys. Rev. Lett.* **83**, 2695 (1999).
- [50] C. J. Pethick and L. P. Pitaevskii, *Phys. Rev. A* **62**, 033609 (2000).
- [51] In the case of effectively repulsive contact interactions, only in one case the state with center-of-mass excitation appears as the state of lowest energy. This is for a finite number of atoms, where the many-body state with $L = 1$ results from center-of-mass excitation of the nonrotating many-body state, with $L = 0$ [49].